Supplementary Material

Interplay of superconductivity and ferromagnetism in ferromagnetic-semiconductor-based Josephson junctions

Hirotaka Hara[1*], Lukas Baker[2*], Axel Leblanc[2], Shingen Miura[1], Keita Ishihara[1], Melissa Mikalsen[2], Patrick J. Strohbeen[2], Jacob Issokson[2], Masaaki Tanaka[1,3,4], Javad Shabani[2, †], and Le Duc Anh[1,3,†]

[1] *Department of Electrical Engineering and Information Systems, The University of Tokyo, Tokyo, Japan*

[2] *Center for Quantum Information Physics, New York University, New York, USA*

[3] *Center for Spintronics Research Network, The University of Tokyo, Tokyo, Japan*

[4] *Institute for Nano Quantum Information Electronics, The University of Tokyo, Tokyo, Japan*

* These authors contribute equally to this work.

[†]Corresponding author: anh@cryst.t.u-tokyo.ac.jp, jshabani@nyu.edu

Superconducting Al thin film properties grown on an InAs/(Ga,Fe)Sb heterostructure

The growth of superconducting Al thin films on ferromagnetic semiconductor (FMS) heterostructures has not yet been well established, therefore, the properties of Al should be carefully examined. Figure S1(a) shows the X-ray diffraction (XRD) pattern of the sample structure presented in Fig. 2(a). Distinct zinc-blende–type GaAs (004) and AlSb (004) peaks are observed at $2\theta = 66.07°$ and 60.12°, respectively. The smaller peak around 61.2° is likely attributable to (Ga,Fe)Sb and InAs. In addition, a face-centered cubic Al (111) peak appears at 38.5°, consistent with the growth orientation identified in the TEM image in Fig. 2(c).

Figures S1(b) and (c) show the electrical transport properties of the Al thin film for evaluation of its superconductivity. Figure S1(b) presents the temperature dependence of the Al resistance, which exhibits a sharp drop at 1.30 K, reaching nearly zero below this temperature. The resistance data shows slight noise, possibly due to measurements during the cooling process. From the transition temperature T_c = 1.30 K, the superconducting gap is estimated as $\Delta_0 = 1.76\, k_B T_c$ = 196 μeV, which agrees well with the value obtained from multiple Andreev reflections in the main text. Figure S1(c) shows the magnetic field dependence of the Al resistance, measured with an in-plane field aligned along the [$\bar{1}$10] direction of the GaAs (001) substrate. The critical field B_c = 1.16 T is comparable to previously reported values [S1]. These results confirm that the Al layer in our sample maintains suitable superconducting properties for observing the proximity effect, even when grown on the FMS heterostructure.

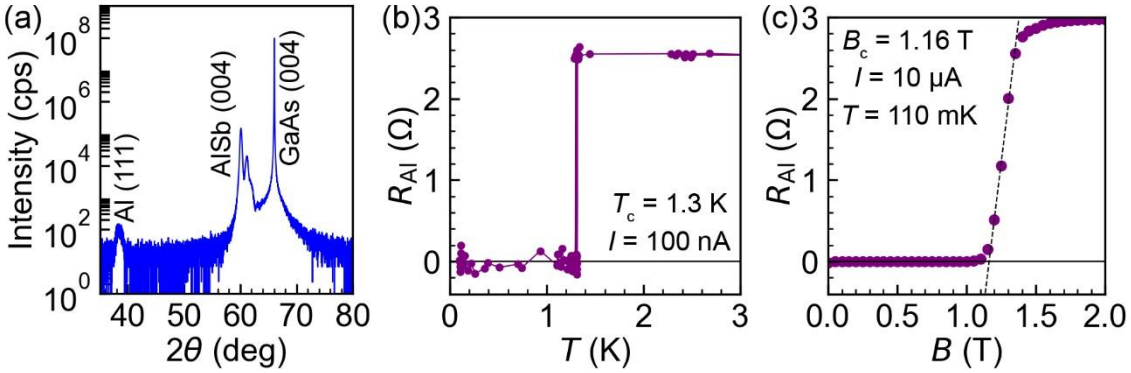

Fig. S1 (a) θ–2θ X-ray diffraction scan of the sample structure shown in Fig. 2(a). (b) Temperature dependence of the Al resistance measured with a current of 100 nA. (c) Magnetic field dependence of the Al resistance. The magnetic field was applied in-plane along the [$\bar{1}$10] direction of the GaAs (001) substrate. The measurement current was 10 μA, and the temperature was 110 mK.

Ferromagnetic properties and calculated stray field generated by (Ga,Fe)Sb

The ferromagnetism of the (Ga,Fe)Sb layer in our sample was evaluated using two techniques, magnetic circular dichroism (MCD) and superconducting quantum interference device (SQUID) magnetometry. Figure S2(a) shows the MCD spectra of (Ga,Fe)Sb measured at 5 K. All spectra obtained under magnetic fields of 1, 0.5, and 0.2 T exhibit identical spectral features at the critical point energies E_1 and $E_1 + \Delta_1$ of GaSb, with no additional peaks. This indicates that the ferromagnetism originates intrinsically from the zinc-blende-type (Ga,Fe)Sb rather than from Fe clusters or secondary Fe-containing compounds.

Figure S2(b) presents an Arrott plot derived from Fig. 2(e), which is an effective method for estimating the Curie temperature T_C from magnetic hysteresis loops [S2]. A positive (negative) intercept of the linear fit corresponds to a ferromagnetic (paramagnetic) state. The intercept crosses the origin at 25 K, indicating that T_C of (Ga,Fe)Sb in this sample is 25 K. This value is lower than those reported in previous studies [S3], likely due to non-optimal growth conditions, as the magnetic properties of FMSs grown by low-temperature MBE are highly sensitive to flux ratios, substrate temperature, and other growth parameters.

Figure S2(c) shows an enlarged hysteresis loop of (Ga,Fe)Sb measured by SQUID (also shown in Fig. 2(e)), exhibiting a remanent magnetisation of approximately 15 emu/cm^3. Using this magnetisation value, the stray magnetic field generated by the (Ga,Fe)Sb layer was calculated at the center of the InAs layer, as shown in Fig. S2(d), to understand its influence on the Josephson junction behaviour under magnetic fields. The calculation was performed based on Maxwell's equations as described in Ref. [S4]. The (Ga,Fe)Sb layer was modeled with dimensions of 30 μm × 5 μm × 20 nm, corresponding to the size of the central electrode in the Josephson junction device. The magnetisation was assumed to be uniaxial and oriented perpendicular to the plane. The calculated results, shown in Fig. S2(e), indicate that the stray field at the InAs layer generated by (Ga,Fe)Sb is perpendicular to the plane and on the order of 0.01–0.1 mT near zero external field. Even when the flux focusing effect arising from the Meissner response of the superconducting electrodes is taken into account, this stray field alone cannot fully explain the magnetic-field positions of the critical-current peaks observed in the Fraunhofer patterns of our junction devices (Fig. 4 (a) and (b)), as discussed in the next section. Nonetheless, the calculated stray field may offer some indication of how magnetic fields influence the superconducting channel.

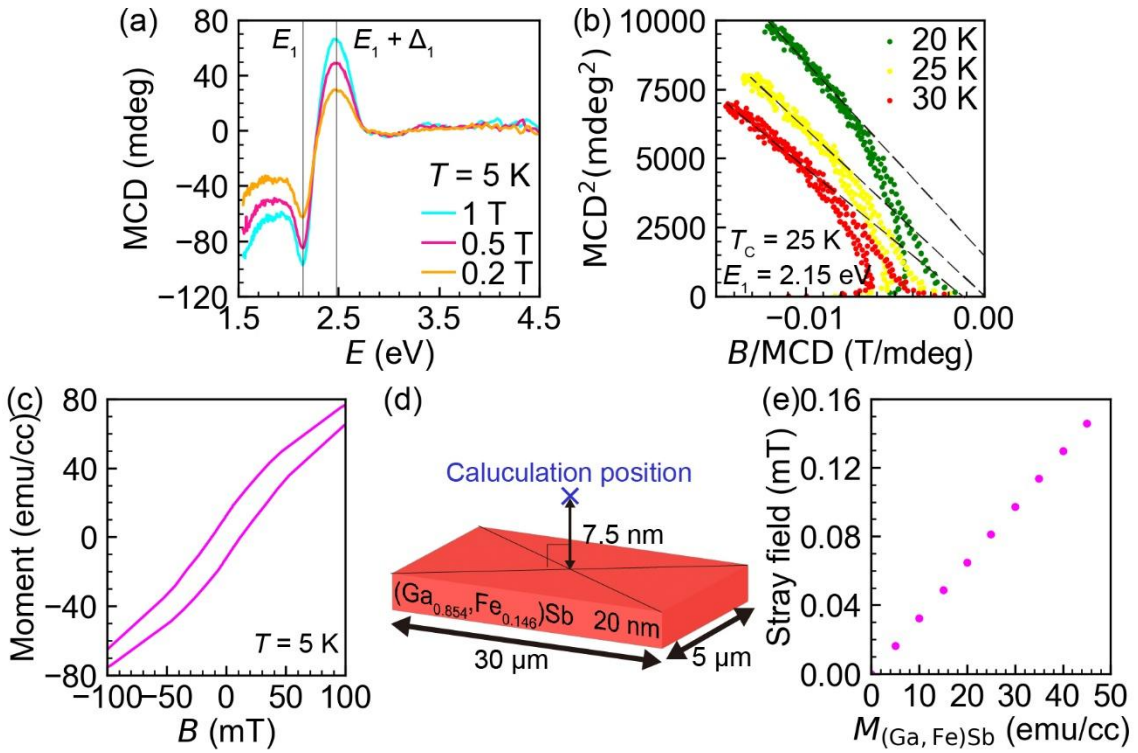

Fig. S2 (a) MCD spectra of (Ga,Fe)Sb measured at 5 K under external magnetic fields of 1, 0.5, and 0.2 T applied perpendicular to the film plane. (b) Arrott plot of (Ga,Fe)Sb obtained at the photon energy E_1 = 2.15 eV. (c) Magnetic hysteresis of (Ga,Fe)Sb measured by SQUID at 5 K when a magnetic field is applied perpendicular to the film plane. (d) Schematic geometry used for calculating the stray magnetic field from (Ga,Fe)Sb at the InAs layer. (e) Calculated stray-field magnitude at the position indicated in (d) as a function of the perpendicular magnetisation of the (Ga,Fe)Sb layer.

Discussion about the magnetic field where the critical current reaches maximum in Fraunhofer patterns

To further understand the Fraunhofer interference observed in the FMS-based Josephson junctions (JJs), it is necessary to examine the magnetic field at which the maximum critical current occurs, denoted B_{shift} in Fig. 4(c). Notably, clear differences appear between Figs. 4 and 5. In Fig. 4, the ungated junction shows its maximum critical current at a field aligned with the initial field, with a magnitude of ~0.4 mT. In contrast, the gated junction (Fig. 5) exhibits the maximum of I_c at a magnetic field opposite to the initial direction, with a magnitude of ~1 mT. This discrepancy raises an unresolved question of what determines the peak positions in the Fraunhofer patterns. Considering the device structure and the possible presence of edge currents, variations in current distribution—potentially arising from differences in the surface conditions of the

junction—may shift the fields at which the critical current peaks appear. Regarding the magnetic properties of (Ga,Fe)Sb, its coercive field is ~20 mT, which cannot account for the observed peak fields. However, the stray field of (Ga,Fe)Sb at the InAs layer with considering flux focusing effect in JJs is calculated to be on the order of 0.1 mT (Fig. S2(e)), comparable but slightly less than the peak positions (~1 mT) observed in Fig. 5 (a)-(e). To fully understand the magnetic field dependence of the critical current peaks, further investigation is necessary through both experimental studies and numerical simulations.

Comparison of gate-voltage dependences of the Josephson critical current and Hall-bar carrier density

Figure S3(a) shows the gate voltage dependence of the critical current I_c in the gated Josephson junction (JJ). The blue data points are extracted from the V–I measurements shown in Fig. 3(f) before applying a magnetic field, while the green points correspond to the maximum I_c values obtained from the Fraunhofer patterns. No I_c data are available between −10 and 0 V from the Fraunhofer measurements due to the measurement procedure; however, we assume that the I_c obtained from the V–I data before applying magnetic field corresponds to the maximum I_c in the Fraunhofer patterns. Indeed, the blue and green data connect smoothly, and these combined data are referred to as peak 1 in Fig. 5(e), (f) in the main text. The junction exhibits a decrease in I_c with increasing the negative gate voltage ($V_{g,\,JJ}$), with saturation observed above 0 V and around −25 V.

Meanwhile, Fig. S3(b) shows the gate voltage ($V_{g,\,Hall}$) dependence of the electron carrier density n measured at 5 K using a gated Hall bar device with a conduction path of 200 μm × 50 μm. n decreases with decreasing the gate voltage and nearly saturates above 10 V and around −30 V, following the same overall trend as in Fig. S3(a). Therefore, the decay ratios of I_c and n are compared in Fig. 5(f) within the gate voltage range where both quantities decrease. The difference in the voltage ranges showing the decay of I_c (−25 to 0 V) and n (−30 to 10 V) may arise from structural differences between the two devices, specifically, the gate-oxide thicknesses (40 nm Al_2O_3 in the JJ device and 100 nm in the Hall-bar device) which were fabricated by different machines or the presence of Al superconducting electrodes in the junction. Thus, we compare the gate-voltage dependence of I_c and n by normalizing the gate voltage range where both the parameters are effectively tuned. The good agreement between the decay ratios of I_c and n likely suggests that the maximum I_c is approximately proportional to n.

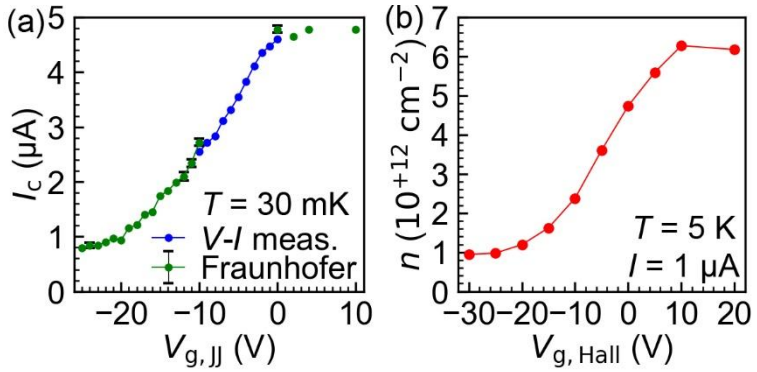

Fig. S3 (a) Gate voltage (V_g) dependence of the critical current I_c in the Josephson junction, obtained from *V-I* measurements before applying an external magnetic field (blue points) and from the maximum values of I_c in the Fraunhofer patterns (green points). (b) Gate voltage dependence of the electron carrier density n measured in a Hall bar device at 5 K with a measurement current of 1 μA.

Fourier-transformation of the Fraunhofer pattern

Analyzing a Fraunhofer interference pattern provides key insights into the Josephson junction, such as the effective area where the supercurrent flows and the spatial distribution of the supercurrent density obtained by fast Fourier transformation (FFT). Figure S4(a) shows the magnetic field dependence of the absolute value of the critical current $|I_c|$ in the same junction as in Fig. 4(c). By comparing I_c^+ (red points) and I_c^- (blue points), a clearly skewed Fraunhofer pattern is observed, which approximately satisfies $I_c^+(+B) \approx I_c^-(-B)$, $I_c^+(+B) \neq I_c^+(-B)$, and $I_c^+(+B) \neq I_c^-(+B)$.

The solid curve in Fig. S4(a) represents a fit using the conventional Fraunhofer interference expression $I_c(B) = I_0 \, |\sin(\pi x)/(\pi x)|$, where $x = \Gamma (B - B_{shift}) \, S / \Phi_0$. Here, Γ is a fitting parameter known as the flux focusing coefficient ($\Gamma = 6.2$), and S is the effective junction area penetrated by the magnetic flux, calculated as $S = W \times (L + 2L_{Al})$, where W = 5 μm is the junction width, L = 100 nm is the junction length, and L_{Al} = 190 nm is the magnetic penetration length into the Al electrodes. The value of L_{Al} was obtained following the method described in Ref. [S5], using $\lambda = \lambda_L(0) \, (1 + \xi/d)^{1/2}$ and $\xi_{thin} = \xi_{bulk}(T_{c,thin}/T_{c,bulk})$, where the parameters are as follows: bulk penetration depth $\lambda_L(0)$ = 16 nm, film thickness d = 10 nm, bulk coherence length ξ_{bulk} = 1.6 μm, experimental $T_{c,thin}$ = 1.3 K, and bulk $T_{c,bulk}$ = 1.2 K [S6][S7]. The large flux focusing coefficient ($\Gamma = 6.2$) indicates that the effective magnetic field in the junction area is approximately six times the external field, likely due to flux concentration arising from the Meissner effect of the Al electrodes and the stray field from the (Ga,Fe)Sb layer.

The supercurrent density distribution in the junction was then calculated by performing a FFT on the data in Fig. S4(a). The coordinate system is defined as follows, x is the current direction, y is the in-plane axis perpendicular to x, and z is the perpendicular direction, as illustrated in Fig. 4(e).

The critical current can be expressed as $I_c(\Gamma\beta)$, where $\beta = 2\pi\ (B-B_{shift})\ (L+2L_{Al})\ /\ \Phi_0$. For the FFT analysis, $I_c(\Gamma\beta)$ is treated as a complex function $F(\Gamma\beta)$, satisfying $I_c(\Gamma\beta) = |F(\Gamma\beta)|$. When $I_c(\Gamma\beta)$ is approximately even with respect to β, it can be written as $F(\Gamma\beta) = I_{c,even}(\Gamma\beta) + iI_{c,odd}(\Gamma\beta)$, where $I_{c,even}$ and $I_{c,odd}$ are the even and odd components of $I_c(\Gamma\beta)$, respectively. The position dependent current density $j(y)$ can then be calculated as $j(y) = \Gamma/(2\pi) \cdot |\int d\beta\ F(\Gamma\beta)\ e^{-i\Gamma\beta y}|$, considering the flux focusing coefficient. The detailed FFT procedure follows Ref. [S8].

The resulting current-density map, shown in Fig. 4(d), reveals that the I_c^+ and I_c^- components in Fig. S4(a) are concentrated near the junction edges, meaningfully larger than the FFT result derived from the ideal Fraunhofer fit. This suggests the presence of conduction channels localised at the two edges of InAs in the junction. The fitted current-density distribution shows a slightly reduced supercurrent density in the junction center, likely due to the limited magnetic field range used in the measurement to avoid flux jumps during field sweeps.

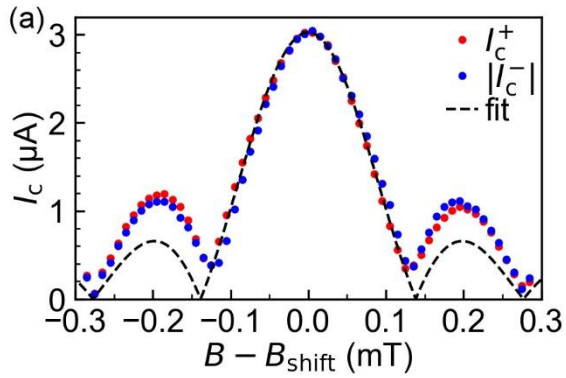

Fig. S4 (a) Magnetic field dependence of the absolute critical current for opposite current directions through the Josephson junction device. The dashed line represents a fit to both I_c^+ and I_c^- using the conventional Fraunhofer interference expression.

In-plane magnetic field dependence of Fraunhofer patterns

We also investigated the dependence of the Fraunhofer patterns on in-plane magnetic fields in the gated Josephson junction to check whether it is a π-junction. Reentrant superconductivity could appear if the junction were to exhibit π-junction behaviour [S9]-[S12]. For clarity in defining the directions of the applied magnetic fields,

a schematic of the gated Josephson junction device and the coordinate axes is shown again in Fig. S5(a). Figure S5(b) shows the critical current I_c as a function of the in-plane magnetic field (parallel to the current) and perpendicular magnetic field, while Fig. S5(d) presents I_c as a function of the in-plane magnetic field (perpendicular to the current) and perpendicular magnetic field. To clearly visualise the maximum I_c, the normalised I_c values for each in-plane field are represented in Figs. S5(c) and S5(e). The perpendicular magnetic field corresponding to the I_c maximum is not stable but fluctuates with the in-plane field, rather than exhibiting clear reentrant superconductivity at a fixed perpendicular field. The fluctuation of the I_c maximum is not likely due to field misalignment, because the fluctuations are not linear with applied field, and is not likely due to measurement instability or noise; variations in magnetic field taking I_c maximum is only 0.2mT, which is much smaller than the observed fluctuations, with multiple scans (5 times) at one in-plane magnetic field. Although the origin of these fluctuations remains unclear, this behaviour possibly represents a feature of Josephson junctions based on FMS heterostructures.

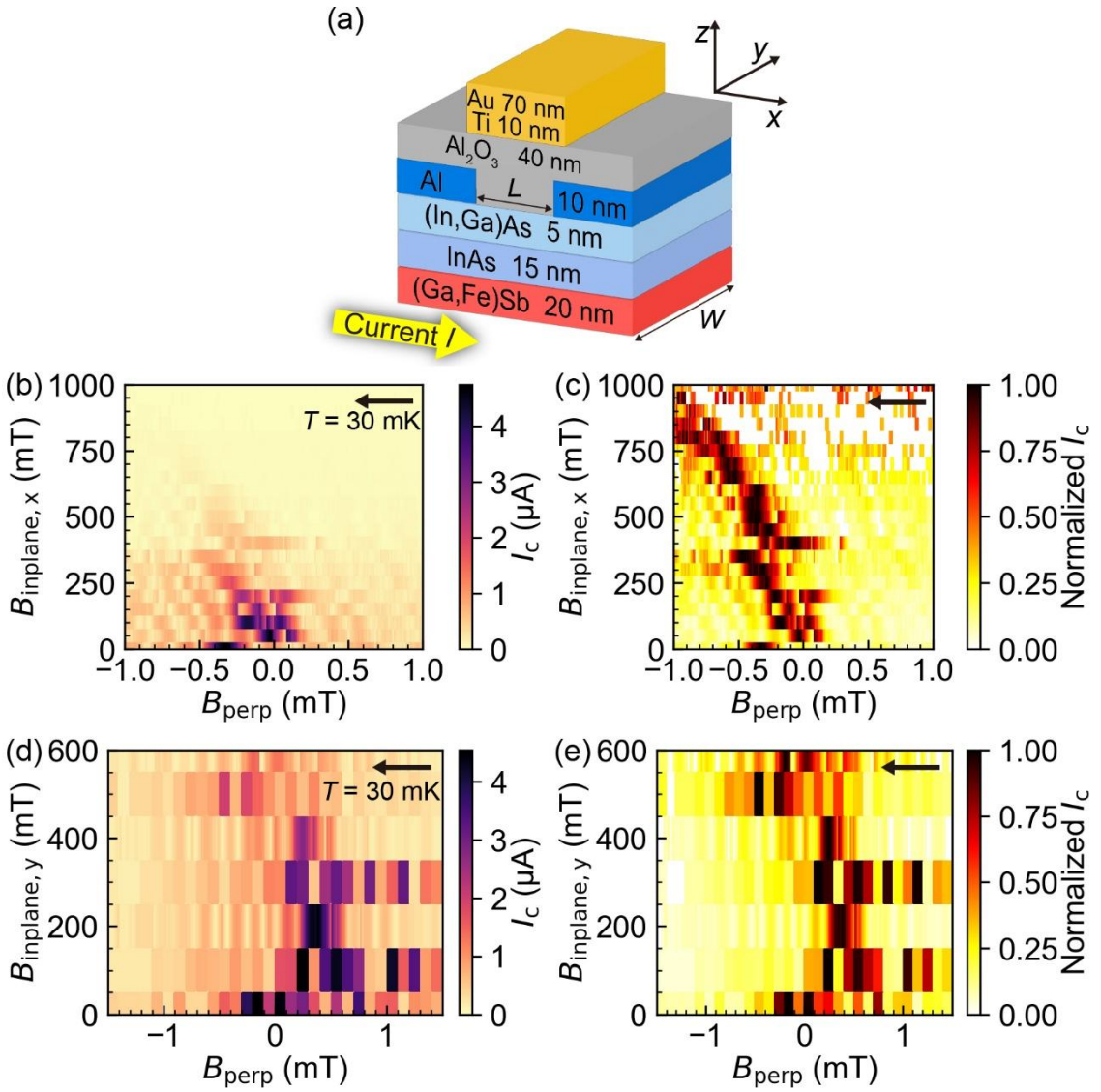

Fig. S5 (a) Schematic illustration of a gated Josephson junction examined in this study and the definition of coordinate axes x, y, and z. (b) Dependence of the critical current I_c on the in-plane (x) and perpendicular (z) magnetic fields. (c) Normalised I_c for each in-plane magnetic field B_x from (b). (d) Dependence of I_c on the in-plane (y) and perpendicular (z) magnetic fields. (e) Normalised I_c for each in-plane magnetic field B_y from (d). Black arrows indicate the sweep directions of the perpendicular magnetic field.

References

[S1] J. Shabani, M. Kjaergaard, H. J. Suominen, Younghyun Kim, F. Nichele, K. Pakrouski, T. Stankevic, R. M. Lutchyn, P. Krogstrup, R. Feidenhans'l, S. Kraemer, C. Nayak, M. Troyer, C. M. Marcus, and C. J. Palmstrøm, "Two-dimensional epitaxial superconductor-semiconductor heterostructures: A platform for topological superconducting networks", Phys. Rev. B 93, 155402 (2016).

[S2] A. Arrott, "Criterion for Ferromagnetism from Observations of Magnetic Isotherms", Phys. Rev. 108, 1394-1396 (1957).

[S3] N. T. Tu, P. N. Hai, L. D. Anh, and M. Tanaka, "Magnetic properties and intrinsic ferromagnetism in (Ga,Fe)Sb ferromagnetic semiconductors", Phys. Rev. B 92, 144403 (2015).

[S4] R. E.-Herbert, and T. Hesjedal, "Calculation of the magnetic stray field of a uniaxial magnetic domain", J. Appl. Phys. 97, 074504 (2005).

[S5] H. J. Suominen, J. Danon, M. Kjaergaard, K. Flensberg, J. Shabani, C. J. Palmstrøm, F. Nichele, and C. M. Marcus, "Anomalous Fraunhofer interference in epitaxial superconductor-semiconductor Josephson junctions", Phys. Rev. B 95, 035307 (2017).

[S6] M. Tinkham, *Introduction to Superconductivity*, 2 ed., Dover Books on Physics (Dover, New York, 2004).

[S7] R. Merservey and B. B. Schwartz, in *Superconductivity*, edited by R. D. Parks (Marcel Dekker, New York, 1969), Vol. 1, p. 126.

[S8] R. C. Dynes, and D. A. Fulton, "Supercurrent Density Distribution in Josephson Junctions", Phys. Rev. B 3, 3015-3023 (1971).

[S9] S. Hart, H. Ren, M. Kosowsky, G. B.-Shach, P. Leubner, C. Brüne, H. Buhmann, L. W. Molenkamp, B. I. Halperin1, and A. Yacoby, "Controlled finite momentum pairing and spatially varying order parameter in proximitized HgTe quantum wells", Nature Phys. 13, 87-93 (2017).

[S10] C. T. Ke, C. M. Moehle, F. K. Vries, C. Thomas, S. Metti, C. R. Guinn, R. Kallaher, M. Lodari, G. Scappucci, T. Wang, R. E. Diaz, G. C. Gardner, M. J. Manfra, and S. Goswami, "Ballistic superconductivity and tunable π–junctions in InSb quantum wells", Nature Commun. 10, 3764 (2019).

[S11] D. Z. Haxell, M. Coraiola, D. Sabonis, M. Hinderling, S. C. t. Kate, E. Cheah, F. Krizek, R. Schott, W. Wegscheider, and Fabrizio Nichele, "Zeeman- and Orbital-Driven Phase Shifts in Planar Josephson Junctions", ACS Nano 17, 18139-18147 (2023).

[S12] P. Mandal, S. Mondal, M. P. Stehno, S. Ilić, F. S. Bergeret, T. M. Klapwijk, C. Gould, and L. W. Molenkamp, "Magnetically tunable supercurrent in dilute magnetic topological insulator-based Josephson junctions", Nature Phys. 20, 984-990 (2024).